The Journal of Chemical Physics

RESEARCH ARTICLE | SEPTEMBER 25 2024

Synthesis and optical properties of perovskite nanocrystals in glass with cationic substitution

Maria S. Kuznetsova ; Elena V. Kolobkova ; Matvey N. Bataev ; Vladimir S. Berdnikov ; Dmitrii V. Pankin ; Mikhail B. Smirnov ; Evgenii V. Ubyivovk ; Ivan V. Ignatiev

Check for updates

J. Chem. Phys. 161, 124501 (2024)
https://doi.org/10.1063/5.0227459

View Online Export Citation

Articles You May Be Interested In

Upconversion properties of Tb 3 + – Yb 3 + codoped fluorophosphate glasses

J. Appl. Phys. (April 2009)

Comparative investigation on the 2.7 μm emission in Er^{3+}/Ho^{3+} codoped fluorophosphate glass

J. Appl. Phys. (November 2011)

Optical properties and energy transfer processes in (Tm 3 + , Nd 3 +) doped tungstate fluorophosphate glass

J. Appl. Phys. (June 2006)

02 October 2024 09:37:45

Challenge us.
What are your needs for periodic signal detection?
Zurich Instruments
Find out more

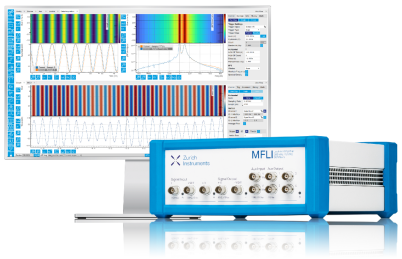

AIP Publishing

The Journal of Chemical Physics ARTICLE pubs.aip.org/aip/jcp

Synthesis and optical properties of perovskite nanocrystals in glass with cationic substitution

Cite as: J. Chem. Phys. 161, 124501 (2024); doi: 10.1063/5.0227459
Submitted: 9 July 2024 • Accepted: 8 September 2024 •
Published Online: 25 September 2024

View Online Export Citation CrossMark

Maria S. Kuznetsova,[1,a] Elena V. Kolobkova,[2,3,b] Matvey N. Bataev,[1,c] Vladimir S. Berdnikov,[1] Dmitrii V. Pankin,[4] Mikhail B. Smirnov,[4] Evgenii V. Ubyivovk,[5,6] and Ivan V. Ignatiev[1,4]

AFFILIATIONS

[1] Spin Optics Laboratory, St. Petersburg State University, 198504 St. Petersburg, Russia
[2] ITMO University, 199034 St. Petersburg, Russia
[3] St. Petersburg State Institute of Technology, 190013 St. Petersburg, Russia
[4] Department of Solid State Physics, St. Petersburg State University, 198504 St. Petersburg, Russia
[5] St. Petersburg State University, 198504 St. Petersburg, Russia
[6] Ioffe Institute, Russian Academy of Sciences, 194021 St. Petersburg, Russia

[a] **Author to whom correspondence should be addressed:** mashakuznecova@bk.ru
[b] kolobok106@rambler.ru
[c] batae1996@gmail.com

02 October 2024 09:37:45

ABSTRACT

The effect of cadmium ions introduced into fluorophosphate glass on the growth and photoluminescence (PL) of the $CsPb_{1-x}Cd_xBr_3$ perovskite nanocrystals (NCs) is systematically studied. The x-ray diffraction patterns have shown that cadmium ions are really incorporated into the NCs that results in a decrease in the lattice constant from 5.85 ($x = 0$) to 5.75 Å ($x = 0.45$). At the large cadmium content in the glass ($x > 0.38$), simultaneous formation of the perovskite $CsPb_{1-x}Cd_xBr_3$ NCs and the non-luminescent $CsCdBr_3$ NCs in the hexagonal phase is found. It is also found that the lattice contraction leads to an increase in the bandgap energy and a noticeable shift of the PL band to the blue region of the spectrum (from 2.42 to 2.68 eV) with a drop in quantum yield from 85% for CsPbBr3 NCs down to 4% for $CsPb0.55Cd0.45Br_3$ NCs. It is shown that the PL quantum yield decreases due to the formation of deep trap states, which manifest themselves as a PL band in the energy range of 1.6–2.5 eV at cryogenic temperatures. A simple model explaining the behavior of the PL band as a function of temperature in the range from 30 to 300 K is proposed.

Published under an exclusive license by AIP Publishing. https://doi.org/10.1063/5.0227459

I. INTRODUCTION

Lead halide perovskites, in particular, all-inorganic colloidal $CsPbX_3$ (X = halide ions) nanocrystals (NCs), are emerging as a family of promising light emitters owing to their size- and composition-dependent tunable bandgap from the violet to near-infrared spectral region.[1–16] In addition, an important advantage of halide perovskites $CsPbX_3$ (X = Br, I) is the stability of their photo-physical characteristics to structural defects.[14] Despite the high density of intrinsic defects, electronic levels in halide perovskites appearing due to point defects are formed within the valence and conduction bands rather than in the bandgap. As a result, the photoluminescence quantum yields (PL QYs) of the colloidal $CsPbBr_3$ and $CsPbI_3$ NCs can reach over 90% in the green and red spectral ranges, respectively. By contrast, $CsPb(Br,Cl)_3$ NCs exhibit much lower PL QYs in the violet-blue region,[17,18] and an insightful understanding of such poor performance remains missing.

To provide blue radiation in the region of 450–480 nm, the modification of the bandgap is required, which could be done by anion[10,19,20] or cation exchange.[20,21] The replacement of lead with lighter ions could produce a blue radiation. However, there is a lack of study of the influence of B-site doping on the optical properties of inorganic perovskite NCs. Based on this motivation, various attempts to exchange Pb^{2+} cations with Sn^{2+}, Ge^{2+}, Cd, Zn, Ni^{2+}, or Bi^{3+} in colloidal $CsPbX_3$ NCs have been undertaken. However, there is no consensus on the efficacy of such substitution. For

Published under an exclusive license by AIP Publishing

example, it was stated in Ref. 20 that the exchange of Pb^{2+} with other cations in $CsPbBr_3$ NCs could lead only to the decomposition of the parent NCs. However, in Refs. 21 and 22, a contrary point of view was expressed. In particular, it was demonstrated that after the prolonged ion exchange, the NCs structure changes completely and the partial exchange of Pb^{2+} with M^{2+} (M = Sn, Cd, and Zn) leads to a blue shift in the PL spectra while maintaining high PL quantum yield (>50%).[21] The blue shift in the optical spectra is explained by the reduction in the lattice constant that accompanies the cation exchange of Pb^{2+} with M^{2+}, yielding doped $CsPb_{1-x}M_xBr_3$ NCs.

In recent years, $CsPbX_3$ NCs doped with various ions (Sn^{2+}, Cd^{2+}, Zn^{2+}, Ni^{2+}, Mn^{2+}, Ln^{3+}, and Bi^{3+}) have been synthesized.[22–35] Doping of the $CsPbX_3$ NCs with these ions leads to the tunability of bandgap[22–25] and removing the nonradiative defect states of the NCs.[26,27]

All the above-mentioned information refers to colloidal nanocrystals. The mechanisms of NCs formation in glasses are fundamentally different from the processes in colloidal chemistry because the introduction of new components in glass composition does not guarantee their incorporation into the crystalline phase. The question arises to what extent the regularities found for colloidal nanocrystals will be repeated during the formation of nanocrystals in glasses. To answer this question, the influence of the bivalent and trivalent ions introduction on the NCs growth process in glasses was investigated. In Refs. 36–45, changes in optical characteristics of the glasses were studied when introducing the same impurity ions into the glass composition. The introduction of M^{2+} and M^{3+} ions into $CsPbBr_3$ NCs have been studied for the borosilicate,[36,40,42] tellurite,[37] borogermanate[41] and germinate[38] glasses. It is argued that all these substitutions improve the photophysical characteristics of the glasses doped with NCs, including an increase in the quantum yield. It should be noted that all the cited studies do not contain information on the concentration of substituted ions in the NCs composition. Only indirect indications of changes in the optical characteristics were present. In particular, it was reported in Ref. 42 that the Cd^{2+} ions were introduced into the $CsPbBr_3$ NCs in the borosilicate glass. The Cd^{2+} doping of the perovskite crystals results in blueshift of the PL and absorption spectra when the concentration of cadmium ions in glass is higher than that of lead.

In our study, the choice of a fluorophosphates (FP) glass host for the formation of $CsPb_{1-x}Cd_xBr_3$ QDs was motivated by the possibility of introducing high concentration of halides and their homogeneous distribution in the glass network, which distinguishes these glasses from the borogermanate, borate, and borosilicate glasses. Previously, we have grown lead-cadmium sulfoselenide NCs in these glasses[43–45] as well as $CsPbX_3$ (X = halide ions) NCs.[46,47] It was found that PL QY of the $CsPbBr_3$ NCs in these glasses is about 85%–90%. A study of the optical and polarization properties of $CsPbX_3$ NCs in FP glass showed their great prospects as materials for photonics and spintronics. In particular, it was shown that NCs with mixed bromine/chlorine anions (the 1:1 ratio) are stable under the influence of laser radiation and magnetic fields, and they do not change their characteristics for a long time.[48,49]

In the present work, the effect of introducing cadmium ions into the glass composition on the growth process of perovskite $CsPb_{1-x}Cd_xBr_3$ NCs and on their luminescence properties was studied. The formation of $CsPb_{1-x}Cd_xBr_3$ NCs in the glass is confirmed by the absorption and PL measurements as well as by the x-ray diffraction (XRD) and transmission electron microscope (TEM) patterns. The dependences of the bandgap shift and PL QY changes on the cadmium ion concentration were obtained. The electronic structure of the NCs in dependence on the cadmium ion content is substantiated.

II. EXPERIMENTAL SECTION

A. Preparation of glass ceramics

Samples of FP glass with composition of $40P_2O_5$–$40BaO$–$20AlF_3$ (mol. %) doped with Cs_2O, PbF_2, CdF_2, and $BaBr_2$ were synthesized using the melt-quench technique. The glass synthesis was performed in a closed glassy carbon crucible at temperature T = 1000 °C. About 50 g of the batch was melted in a crucible for 30 min and then the glass melt was cast on a glassy carbon plate and pressed to form a plate with a thickness of about 2 mm and a diameter of 7–8 cm. The samples were annealed at a temperature of 50 °C below glass transition temperature (T_g = 400 °C). The $CsPb_{1-x}Cd_xBr_3$ perovskite NCs were precipitated by the glass self-crystallization during melt-quenching and additional heat treatment at 420 °C for 30–60 min.

B. Experimental methods

Differential scanning calorimeter STA 449F1 Jupiter Nietzsche was used for measurement of the glass transition temperature (T_g). The studies of glass chemical composition were performed by scanning electron microscopy (SEM, Tescan Vega 3 SBH, Czech Republic) with energy-dispersive x-ray spectroscopy (EDX).

The precipitation of $CsPbBr_3$ NCs in FP glass was identified with the x-ray diffraction (XRD) method. Diffraction patterns were recorded with a Rigaku X-ray diffractometer using $Cu_{K\alpha}$ radiation. The x-ray diffraction was detected in the double angle range from 10° to 80° in the Bragg–Brentano geometry. A 0.02 mm thick Ni foil was applied to suppress Cu K_β radiation. The measurement step was 0.05°. The identification was performed using the PDWin 3.0 software package. The search of analogs was carried out within the ICDD PDF-2 database of powder x-ray diffraction patterns.

To estimate the shape, the average size, and the size distribution of the NCs after the exchange $Cd^{2+} \rightarrow Pb^{2+}$, we used the scanning transmission electron microscope Zeiss Libra 200FE (TEM). The absorption spectra of the FP glass samples at room temperature were recorded in the 200–800 nm spectral region using a Lambda 650 PerkinElmer spectrophotometer.

Temperature-dependent PL measurements were carried out in the temperature range of 10–300 K. To study the PL, we used the standard technique of the continuous-wave (CW) spectroscopy. The experimental setup was equipped with a helium closed-cycle cryostat, which made it possible to vary the temperature of the sample in the range from 10 to 300 K. For the non-resonant PL excitation, a diode laser with the photon energy E_{exc} = 3.06 eV was used. The laser radiation was focused into a 50 μm aperture and then refocused on the sample using a short-focus lens into a spot with a diameter of 40 μm. The PL was collected in backward geometry. The laser excitation was incident onto the sample at a small

02 October 2024 09:37:45

Published under an exclusive license by AIP Publishing

angle to the of the optical axis, so that the reflected beam did not enter the lens aperture in the PL collection channel on a slit of the IHR-550 spectrometer (focal length 550 mm, diffraction grating 600 grooves per mm). The spectrometer was equipped with a Symphony II CCD camera cooled with liquid nitrogen, which ensured a low noise level.

The absolute quantum yield was measured with an Absolute PL Quantum Yield Measurement System C9920-02G, −03G (Hamamatsu) consisting of a PMA-12 Photonic multichannel analyzer with an InGaAs sensor (200–950 nm range with 2 nm resolution), an A10104-01 integrating sphere unit, a monochromatic light source L9799-01 with a 150 W Xenon light source, and a remote-controlled monochromator (250–950 nm range, bandwidth from 2 to 5 nm).

III. RESULTS AND DISCUSSION

In recent years, the possibility of exchanging Pb^{2+} for another cation has been investigated for colloidal NCs using either *in situ* incorporation of guest cations during the particle growth or applying a post synthesis treatment. The latter is generally carried out at low temperatures, having the advantage of avoiding thermally activated out-diffusion of the guest species. In addition, van der Stam *et al.*[21] have showed that the post synthesis $Cd^{2+} \rightarrow Pb^{2}$ exchange $^{+}$in NCs results in an increase in E_g and, correspondingly, in the PL energy shift to the blue spectrum region without losses of the PL QY.

Unfortunately, the crystallization process in multicomponent glasses is complex, and there is no reason to assume that the introduction of impurity ions necessarily leads to their incorporation into the NC structure. These impurities can be embedded into the glass network, while the crystal phase remains unchanged. This property has a fundamental difference between the crystallization process in glasses and the mechanism of the colloidal NCs formation by a chemical assembly. Glasses usually contain a large number of components, and there is no reason to expect that the impurities that are involved in the formation of colloidal NCs will behave similarly in glasses. Evidence of impurity incorporation into the NC structure may be only the shift in the peak position in the x-ray diffraction pattern.

A. Composition and physical properties

In our technological experiments, the concentration of lead fluoride (PbF_2) was a constant value of 7.5 mol. %. The concentration of cadmium fluoride (CdF_2) varied from 0.75 to 8.5 mol. %. The specified substitution kept the glass transition temperature and coefficient of thermal expansion (CTE) practically unchanged and amounted 390–400 °C and 145 × 10^{-7} K^{-1}, correspondingly. For analysis of the influence of the introduction of cadmium ions in the composition of fluorophosphate glass, the ratios of CdF_2/PbF_2 (mol. %) 1/10, 2/10, 3/10, 5/10, 6/10, 7/10, and 12/10 were used. In recalculation on mole fractions of PbF_2 and CdF_2, they correspond to the expected NCs composition (initial composition) in the glass samples presented in Table I. The real compositions of glasses were obtained by energy-dispersive x-ray spectroscopy (EDX).

B. TEM and XRD study

To estimate the shape, the average size, and the size distribution of NCs after the exchange $Cd^{2+} \rightarrow Pb^{2+}$, we used the scanning transmission electron microscope Zeiss Libra 200FE. Because the highly resistive glass samples become charged by the electron beam, they require preliminary preparation before measurements of the TEM images. The glass sample was ground into powder in an agate mortar. The powder was placed into an ultrasonic bath and then on a carbon-coated copper grid. Figure 1(a) shows the TEM image for one of the pieces, which allowed us to observe the NCs in the glass. Using the calibrated ruler, we have obtained the histogram of the NCs sizes [Fig. 1(b)]. The average size of the NCs obtained from this histogram is (12.6 ± 1) nm. The average size of NCs is larger than the exciton Bohr radius. Correspondingly, the quantum confinement effect does not significantly contribute to the energy shift of optical transitions.

The average size of NCs can also be determined from the XRD measurements using the Scherrer formula for a peak at 31°. (see Fig. 2). The Scherrer equation can be written as $d = K\lambda/(\beta \cos\theta)$, where K is a dimensionless shape factor equal to 0.9, λ is the x-ray wavelength, β is the line broadening (full width at the half maximum, FWHM) in radians, and θ is the Bragg angle. From the analysis of the XRD patterns, the NCs size of 13 ± 1 nm was obtained. The sizes

TABLE I. Compositions of glasses with variable cadmium concentration based on the energy-dispersive x-ray spectroscopy (EDX) and their designation.

Initial composition	CdF_2/PbF_2 atomic ratio	Real concentration (at. %)									
		O	F	Cd	Al	P	Br	Cs	Ba	Pb	Amount (at. %)
$CsPb_{0.91}$ $Cd_{0.09}Br_3$	1/10	63.38	8.18	0.11	1.79	15.62	0.85	1.67	8.38	1.09	100.00
$CsPb_{0.83}$ $Cd_{0.17}Br_3$	2/10	62.31	8.48	0.10	1.83	15.55	0.85	1.67	8.38	1.09	100.00
$CsPb_{0.77}$ $Cd_{0.23}Br_3$	3/10	61.70	8.35	0.5	1.81	15.16	1.00	1.67	8.11	1.02	100.00
$CsPb_{0.67}Cd_{0.33}Br_3$	5/10	62.90	7.80	0.62	1.04	15.64	0.88	1.75	8.42	1.03	100.00
$CsPb_{0.62}Cd_{0.38}Br_3$	6/10	60.54	9.31	0.8	1.67	14.90	0.88	1.63	7.82	0.96	100.00
$CsPb_{0.55}Cd_{0.45}Br_3$	8/10	60.54	9.31	0.7	1.67	14.90	0.88	1.63	7.82	0.96	100.00
$CsPb_{0.45}Cd_{0.55}Br_3$	12/10	62.1	8.2	1.4	1.5	15.3	0.85	1.71	8.0	1.02	100.00

02 October 2024 09:37:45

Published under an exclusive license by AIP Publishing

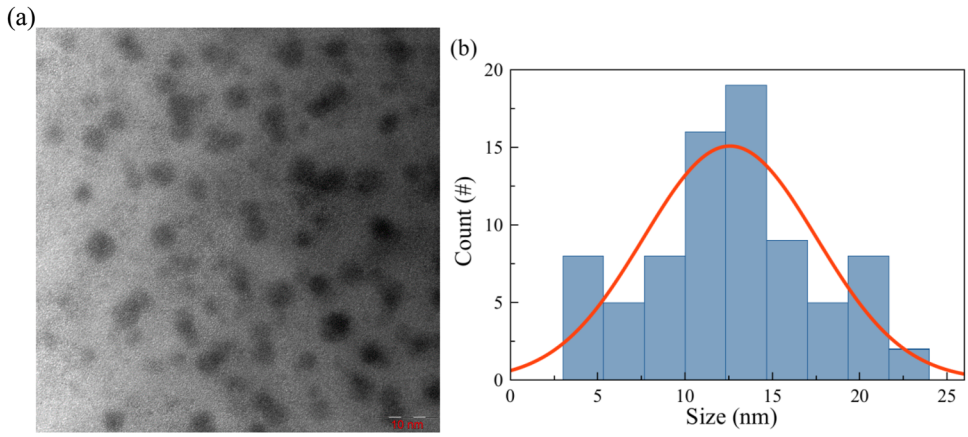

FIG. 1. (a) TEM image for a small piece of the glass containing NCs. The NCs are visible as black spots in the image. (b) The obtained histogram of the NC sizes resulting in the average NC size of 12.6 nm.

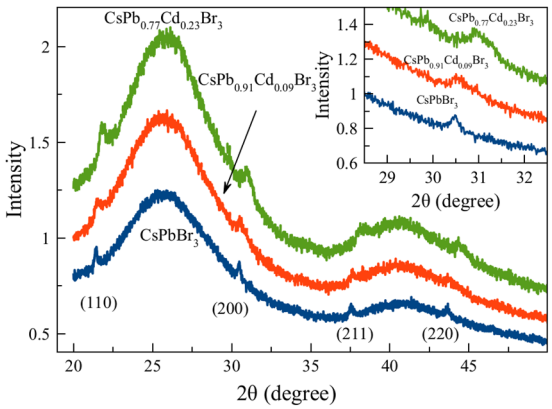

FIG. 2. XRD patterns of the glass sample with $CsPbBr_3$ (JCPDS No. 01-072-7929) and glass samples with CdF_2/PbF_2 ratio of 1/10 and 3/10. The inset shows the second diffraction peak in a magnified scale.

evaluated from the TEM and XRD measurements coincide within experimental errors.

Figure 2 shows the x-ray patterns of a glass without Cd implantation and two FP glasses with different CdF_2 content, in which the NCs were formed after additional heat treatment at 420 °C during 1 h. The results show that the NCs are successfully formed in the glasses. The diffraction pattern of glasses with NCs $CsPbBr_3$ shows four main peaks at double angle, $2\theta = 21.5°$, 30.5°, 37.5°, and 43.6°. As shown in the inset of Fig. 2, the position of the XRD peaks shifts to the larger angles when the Cd^{2+} concentration in the glass increases up to CdF_2/PbF_2 ratio of 3/10. The patterns at such angles are characterized by both the cubic phase (PDF#75-0412) and orthorhombic phase (JCPDS No. 01-072-7929) of bromide perovskite. In the cubic phase, such angles correspond to the following Miller indices: (110), (200), (211), and (220). At the orthorhombic phase, it corresponds to the (112), (220), (312), and (224) Miller indices. The small concentration of NCs does not allow us to determine the perovskite phase accurately due to the coincidence of intense peaks of high (cubic) and low-temperature (orthorhombic) phases.

We also analyzed the XRD patterns for the nanocrystalline phase obtained in the glass samples with the Cd/Pb ratios of 6/10 [Fig. 3(a)] and 12/10 [Fig. 3(b)].

The x-ray diffraction pattern of glass with a large Cd/Pb ratio of 6/10 contains additional peaks in the range of 28°–30°; see Fig. 3(a). This indicates the release of a new, non-perovskite, crystalline phase of $CsCdBr_3$ NCs (PDF Card No. 00-024-023). Simultaneously, the peaks corresponding to the perovskite Cs(Pb, Cd)Br_3 NCs shift to smaller angles. This points out to the decrease in the cadmium concentration in these NCs. A similar effect was observed in Ref. 21. Further increase in Cd^{2+} concentration in the glass composition leads to the formation of only $CsCdBr_3$ NCs in a hexagonal form [Fig. 3(b)]. These observations allow us to conclude that the Cd/Pb = 3/10 cation ratio (glass $CsPb_{0.77}Cd_{0.23}Br_3$) is the upper limit for the formation of only the perovskite NCs.

When Cd^{2+} ions enter the $CsPbBr_3$ lattice, the successful replacement of Pb^{2+} ions leads to lattice shrinkage. This agrees with the results of calculations using Bragg's law.[21] Analysis of the x-ray diffraction patterns shows that the atomic reflexes are shifted to larger scattering vectors for the glasses containing CdF_2. This fact indicates that the atomic lattice of $CsPbBr_3$ shrinks when the small Cd^{2+} guest cations are incorporated in the NCs (Fig. 4). This is the expected result because the ionic radius of Pb^{2+} [$R(Pb^{2+})$ = 1.19 Å] is significantly larger than that of the guest divalent cation [$R(Cd^{2+})$ = 0.95 Å]. The average lattice parameter can be determined by Bragg's law: $a = d\sqrt{k^2 + l^2 + h^2}$, where $d = n\lambda/(2\sin\theta)$ is the spacing between diffracting planes. Here $\lambda_{CuK\alpha 1}$ = 1.540 59 Å; *k, l, and h* are the Miller indices; and θ is the diffraction angle.

The lattice parameter of $CsPbBr_3$ and $CsCdBr_3$ was taken from the literature for the cubic perovskite structure.[21,50,51] To determine x in $CsPb_{1-x}Cd_xBr_3$ NCs, linear interpolation has been used between the lattice constants a for the cubic phase of $CsPbBr_3$ (a = 5.849 Å) and $CsCdBr_3$ a = 5.62 Å. We found that the lattice constant decreases from a = 5.849 Å for pure $CsPbBr_3$ NCs down to a = 5.81 Å for

02 October 2024 09:37:45

Published under an exclusive license by AIP Publishing

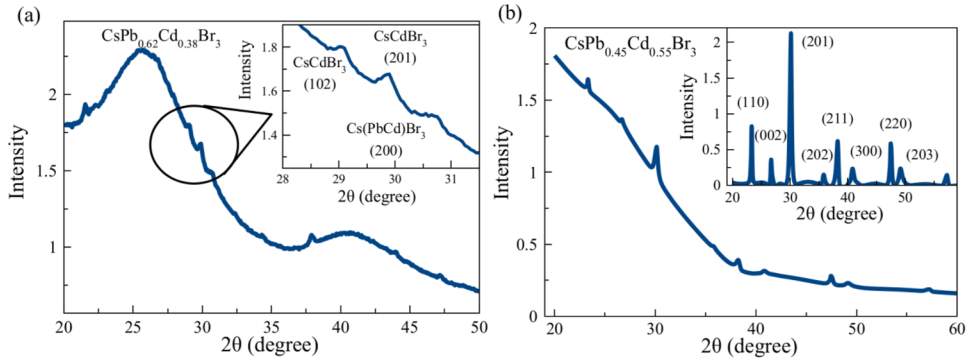

FIG. 3. (a) XRD patterns of the glass doped with CdF_2/PbF_2 ratio of 6/10. The inset shows a fragment of the XRD pattern in the magnified scale in the region of additional peaks. (b) XRD patterns of the glass doped with CdF_2/PbF_2 ratio of 12/10. The inset shows the XRD patterns after the background subtraction.

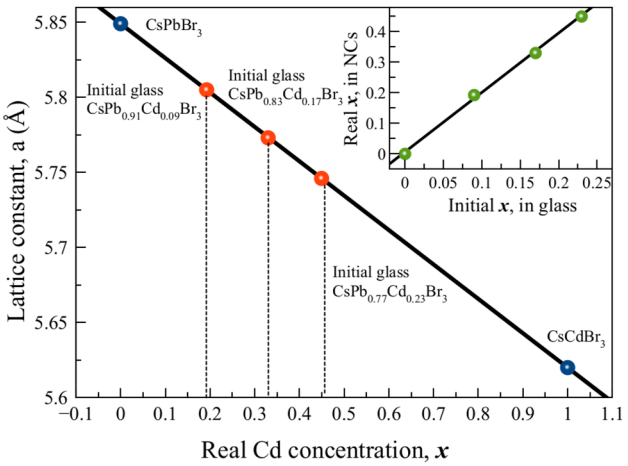

FIG. 4. Dependence of the $CsPb_{1-x}Cd_xBr_3$ lattice parameter on Cd^{2+} ion concentration in NCs based on linear interpolation between $CsCdBr_3$ and $CsPbBr_3$ parameters. The inset shows the relation between the Cd^{2+} concentration introduced into the glass and the Cd^{2+} concentration in the NCs.

NCs in glass with the Cd/Pb ratio = 1/10 and 5.75 Å for glass with the Cd/Pb ratio = 3/10. Using these data and the linear interpolation, we can determine the real concentration of Cd in NCs (see Fig. 4). In particular, NC compositions are $CsPb_{0.81}Cd_{0.19}Br_3$ for the glass with Cd/Pb ratio = 1/10, $CsPb_{0.67}Cd_{0.33}Br_3$ for the glass with Cd/Pb ratio = 2/10, and $CsPb_{0.55}Cd_{0.45}Br_3$ for the glass with Cd/Pb ratio = 3/10. As shown, the Cd/Pb ratio in NCs is significantly larger that the initial Cd/Pb ratio in the studied glass samples, as shown in the inset in Fig. 4. The obtained results allow us to conclude that the real composition $CsPb_{0.55}Cd_{0.45}Br_3$ is the upper limiting value of the cadmium ion concentration in NCs.

To confirm the above-mentioned assumption about the linear dependence of the lattice constant on the concentration of Cd, the theoretical calculations of the lattice constants of CsPbBr3, CsCdBr3, and $CsCd_{1-x}Pb_xBr_3$ solid solution were carried out. The calculations were performed in the framework of generalized gradient approximation (GGA) of the density functional theory (DFT) with the Perdew–Burke–Ernzerhoff (PBE) functional and the norm-conserving pseudopotential in CASTEP software (Material Studio).[52,53] The cutoff energy value for constructing the plane wave basis was chosen as 1200 eV. For the electronic structure calculations, the self-consistency field (SCF) criterion was set to 5×10^{-8} eV/atom. Geometry optimization was performed using the modified Broyden–Fletcher–Goldfarb–Shanno LBFGS method[54] until residual forces, residual stresses, and maximum ionic displacements, which did not exceed 0.005 eV/Å, 2×10^{-4} GPa, and 5×10^{-5} Å, respectively. The k-space integration grid was chosen according to the Monkhorst–Pack scheme.[55] The dimension of the k-space grid was chosen to be $4 \times 4 \times 4$ for $CsPbBr_3$ and $CsCdBr_3$, which provided the step about 0.043 1/Å. The convergence of properties was also checked when calculating with a $6 \times 6 \times 6$ grid.

To simulate the $CsCd_{0.5}Pb_{0.5}Br_3$ solid solution, a supercell was created with double the dimensions of the original cell, i.e., $2 \times 2 \times 2$. The dimension of the k-space grid in this case was chosen to be $2 \times 2 \times 2$. This was done to ensure that the steps in k-space were the same for all the calculations. The replacement of Pb atoms with Cd atoms was carried out so that the symmetry of the supercell remained the same as the symmetry of the crystals. In all the cases, the space group was $Pm\bar{3}m$ (No. 221). The results of the calculations show that the linear dependence of the lattice constant as a function of the concentration x of Cd is really observed that confirms the approximation used in Fig. 4.

The results presented above clearly show that guest cations, Cd^{2+}, can be incorporated into $CsPbBr_3$ NCs during crystal growth from the melt. The results obtained show a significant discrepancy in the injected Cd/Pb ratio and the Cd/Pb ratio in the grown NCs. On the basis of these results, we conclude that guest divalent cations are indeed present in the perovskite NCs and are distributed homogeneously across the perovskite lattice. However, as it was concluded in Ref. 21 for a series of $CsPb_{1-x}Cd_xBr_3$ colloidal NCs, no continuous series of solid solutions occurs and $x = 0.1$ is the limiting value of the concentration of cadmium ions. For $CsPb_{0.9}Cd_{0.1}Br_3$ colloidal NCs, the value of the lattice constant $a = 5.70$ Å was determined.

02 October 2024 09:37:45

Published under an exclusive license by AIP Publishing

Differences in the determination of cadmium ion concentration in the colloidal NCs[21] and our results are most probably related to the peculiarity of ion exchange during the colloidal synthesis. It is well known that the ion exchange results in an inhomogeneous distribution of the cadmium ions along the depth. Its concentration exponentially decreases from the surface to the NC center. Luminescence is caused by the surface of the NC with a high concentration of cadmium ions, while the average concentration of cadmium ions is much smaller.

C. Luminescent properties at room temperature

The optical properties of $CsPb_{1-x}Cd_xBr_3$ NCs in the PF glass were studied in detail. Figure 5 shows the PL and transmission spectra of all the samples under study measured at room temperature (T = 300 K). As shown in Fig. 5(a), the PL peak position of $CsPbBr_3$ NCs and of $CsPb_{1-x}Cd_xBr_3$ NCs with different concentrations of Cd^{2+} ions shifts from E = 2.42 eV for the *pure* $CsPbBr_3$ NCs (no Cd^{2+} ions) to E = 2.68 eV with an increasing Cd^{2+} content up to 3/10. We should note that the PL band, even in the pure $CsPbBr_3$ NCs, is shifted to the higher energy relative to that for the bulk $CsPbBr_3$ crystal (E = 2.32 eV[56]), which is due to the spatial confinement effect in the NCs.

The contraction of the perovskite crystal cell leads to increasing interaction between the lead and bromine orbitals resulting in a blueshift in the luminescence spectrum.[21] It should be noted that the luminescence band of colloidal $CsPbBr_3$ NCs (E_{max} = 2.42 eV) shifts after the Cd^{2+} exchange to E_{max} = 2.74 eV, which corresponds to the energy shift of 0.32 eV.[21] For $CsPbBr_3$ NCs of the same size in the glass matrix, the PL band maximum shifts by about 0.26 eV after the Cd^{2+} exchange. The transmission spectrum edge shifts from 2.6 eV for the pure $CsPbBr_3$ NCs to 2.77 eV for the Cd^{2+} content 3/10 [see the inset in Fig. 5(a)].

The transmission spectra for the samples with a large concentration of Cd^{2+} (the Cd/Pb content ratio is 5/10 and 6/10) shift to the opposite direction. Similar behavior is also observed for the PL bands of these samples. This behavior of optical spectra points out that the Cd concentration in NCs *decreases*, rather than increases, when the initial Cd/Pb content ratio in the glass becomes too large. We assume that the non-luminescent $CsCdBr_3$ NCs are formed at such content ratio. This assumption is supported by the XRD date shown in Fig. 3. The Cd ions are spent mainly on the formation of such NCs and only a small fraction of Cd ions is incorporated in the perovskite $CsPb_{1-x}Cd_xBr_3$ NCs. This process causes the reduction of the PL QY observed for the glass samples with large content ratios of 5/10 and 6/10.

The real Cd ions concentration x in the perovskite NCs can be evaluated from the energies of the PL and absorption bands. The left inset in Fig. 5(a) shows the dependence of the exciton energy on the concentration x. It is obtained using XRD data for three samples (see Fig. 3). The dependence is linear within the experimental errors. It can be used to find the Cd ions concentration from optical spectra of other samples, which are not characterized by XRD. We should note that the XRD characterization is problematic when the fraction of the perovskite NCs becomes small, in particular for the glass samples with the initial Cd/Pb ratios of 5/10 and 6/10. The Cd ions concentrations obtained by this way are shown in Fig. 5(a).

The experimental data shown in Fig. 5(b) allow one to evaluate the fraction K of perovskite NCs in the samples with high Cd/Pb ratios. We suppose that in the glass samples with initial Cd/Pb ratio up to 3/10, all the NCs (100%) are formed in the perovskite phase and the decrease in the PL yield ($QY^{(0)}$) is caused by the defects induced by Cd ions. The dependence $QY^{(0)}(x)$ is well approximated by a phenomenological function shown in Fig. 5(b). Further decrease in the PL yield (QY) for the glass samples with larger Cd/Pb ratio (see the bottom experimental points x = 0.33 and x = 0.08) is due a decrease in fraction K of the perovskite NCs. Therefore, we suppose that $K = QY/QY^{(0)}$. Using the data shown in Fig. 5(b), we obtain: K = 0.44 for the glass with the Cd/Pb ratio of 5/10 (x = 0.33) and K = 0.074 for the ratio of 6/10 (x = 0.08).

The observed effect of cadmium ions on the luminescence characteristics of NCs should be compared to previously reported data.[21,42,52] The authors of Ref. 21 state that after the cadmium

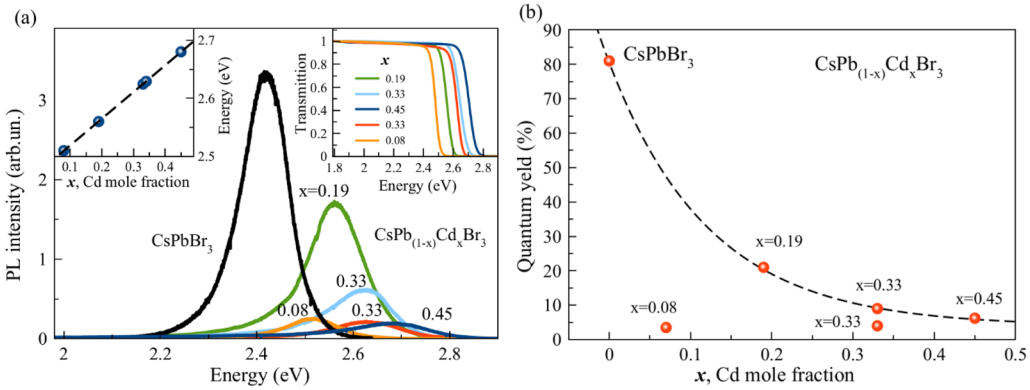

FIG. 5. (a) PL spectra of glass doped with $CsPbBr_3$ and $CsPb_{1-x}Cd_xBr_3$ NCs. The left inset shows a relation between the Cd^{2+} concentration in the NCs and the energy of the PL peak. The right inset shows the transmission spectra for these samples. (b) Dependence of quantum yield on the Cd^{2+} concentration in the NCs. The dashed curve is the approximation by function, $y = a\exp(-x/b) + d$, with a = 77%, b = 0.12, and d = 4%.

02 October 2024 09:37:45

Published under an exclusive license by AIP Publishing

ions introduction, the quantum yield decreases insignificantly from 90% to 50%. In Ref. 42, a PL shift to 2.64 eV was observed for $CsPb_{0.7}Cd_{0.3}Br_3$ NCs in a borosilicate glass. It was found that the fluorescence intensity of Cd^{2+} doped $CsPbBr_3$ NCs in borosilicate glass significantly increases after doping with a low concentration of Cd^{2+}, reaches a maximum at the ratio lead/cadmium of 3, and then decreases. The authors have concluded that the fluorescence intensity of $CsPbBr_3$ NCs can be really enhanced by the Cd^{2+} doping.[42] However, the absence of a spectral shift of the PL band in the range of Cd/Pb concentrations from 0 to 0.3/0.7 in Ref. 42 indicates the formation of NCs containing no cadmium ions. Accordingly, the PL QY change is caused, most probably, with an improvement in the structure of $CsPbBr_3$ NCs.

In Ref. 52, it was shown that the stability and PL QY of colloidal $CsPbX_3$ NCs can be enhanced by the CdX_2 post-treatment. The reaction mechanism during the post-treatment of CdX_2 was studied by means of PL spectra, XRD patterns, and XPS spectra. It was found that the benefits of the CdX_2 post-treatment are not only that the halide ions are beneficial to improve the properties of NCs but also the presence of Cd^{2+} helps to reduce the number of surface defects and improves the optical stability of the samples.

The results obtained in our work contradict those reported in the papers cited above. We have found that the incorporation of cadmium ions into NCs leads to a decrease in PL QY at room temperature. If the calibration of the Cd/Pb compositions is correct, the introduction of even relatively small Cd concentration reduces the PL QY from 80% for pure $CsPbBr_3$ down to 21% for $CsPb_{0.81}Cd_{0.19}Br_3$ [Fig. 5(b)].

In Ref. 32, it was noted that replacing Pb^{2+} with other metal ions may bring new deep defect states, destroying the defect tolerance nature of the host $CsPbBr_3$. These new defect states may act as traps and scattering centers hampering the optoelectronic performance. It is known that the occurrence of trapped states should lead to a decrease in the quantum yield. In our work, the PL spectra at low temperatures were studied to understand the reasons for the strong decrease in the PL QY at room temperature.

D. Low temperature PL

We measured the low-temperature PL spectra for all the samples under study. Figure 6 shows the PL spectra measured at temperature T = 11 K for samples with the $CsPbBr_3$ NCs and with the $CsPb_{(1-x)}Cd_xBr_3$ NCs containing different Cd content, Cd/Pb = 1/10, 2/10, and 3/10. It is shown in Fig. 6 that all the PL spectra contain the main exciton peak (the X band) at the energy of about 2.4 eV for the $CsPbBr_3$ NCs, which shifts to higher energies with increasing of the Cd^{2+} content. In addition, an additional wide PL band (the A band) appears in the energy range of 1.6–2.5 eV when the Cd^{2+} ions are incorporated in the NCs. The intensity of this band rises with increasing the Cd^{2+} concentration. This behavior is opposite to that of the intensity of the exciton peak, which decreases with increasing Cd concentration. Obviously, this broad band is associated with the occurrence of trapped states located in the bandgap of these materials.

The presence of trapped states can be verified by studying the PL spectra at different excitation powers. Figure 7 shows examples of the PL spectra measured for the sample $CsPb_{1-x}Cd_xBr_3$ with

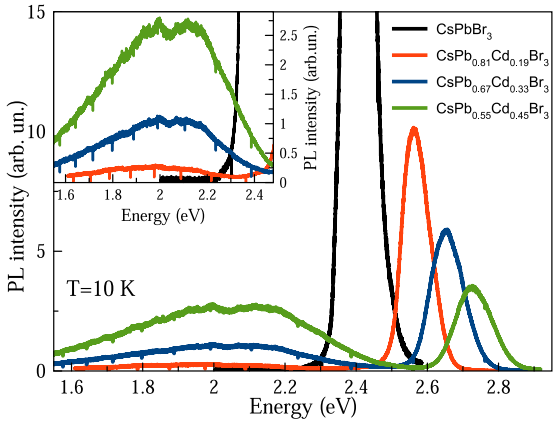

FIG. 6. PL spectra of samples $CsPb_{(1-x)}Cd_xBr_3$, with x = 0, 0.19, 0.33, and 0.45. The inset shows the additional band in an enlarged scale.

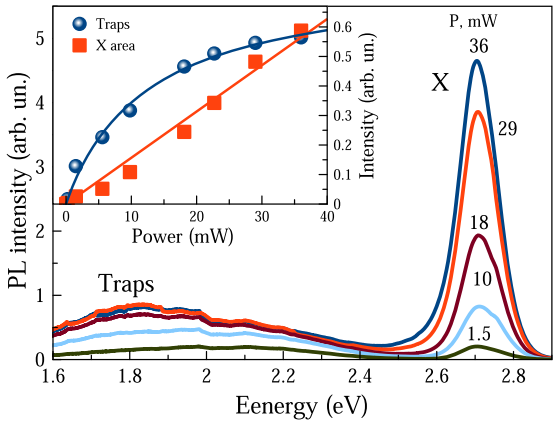

FIG. 7. Power dependence of the PL spectra of samples $CsPb_{1-x}Cd_xBr_3$ with x = 0.45. The inset shows the power dependences of integral intensities of the exciton band (X, red rhombus) and the wide band (Traps, blue points). The solid red line is the linear fit, and the blue curve is the fit by Eq. (1) with parameter P_0 = 12.4 mW. T = 11 K.

x = 0.45. The inset in this figure demonstrates the power dependence of the integral intensities of the X and A bands. As can be seen, the intensity of the exciton band depends approximately linearly on the power in the power range used in these experiments. At the same time, the integral intensity of the A band tends to saturate at a sufficiently high power. Such behavior point out to the limited number of traps localized within each NC. These traps can be populated by excited carriers that block further increase in the PL of the A band. A simple analysis of a rate equation shows (see, e.g., Ref. 57) that the integral intensity of the PL band can be approximated by the expression,

$$I_A(P) = A\frac{P}{P + P_0}. \quad (1)$$

02 October 2024 09:37:45

Published under an exclusive license by AIP Publishing

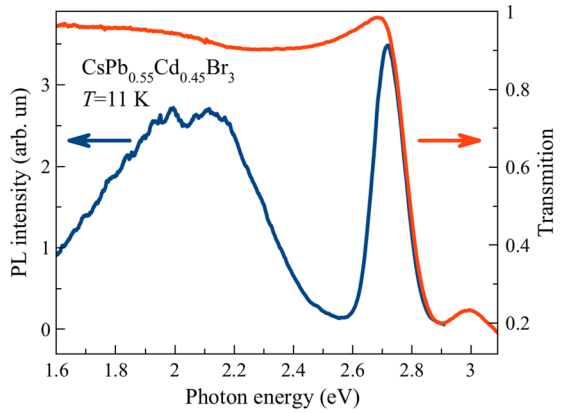

FIG. 8. PL (blue curve) and transmission (red curve) spectra of the sample $CsPb_{0.55}Cd_{0.45}Br_3$.

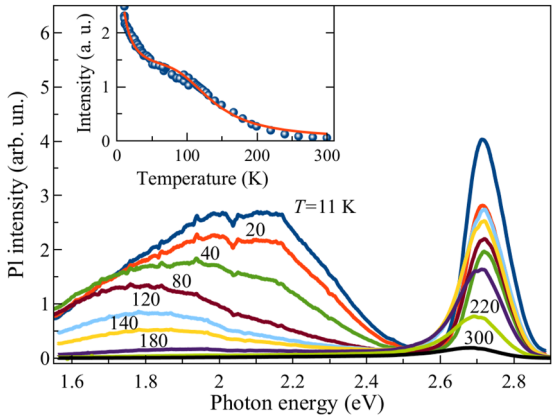

FIG. 9. Temperature dependence of PL spectra of the $CsPb_{0.55}Cd_{0.45}Br_3$ sample. The inset shows the integral intensity of the PL as a function of temperature (symbols) and the fit by Eq. (2) (red curve).

Here, A is a scaling factor and P_0 is a characteristic power. It is determined by the density of traps, N_c, and the lifetime of the photocreated carrier, τ_c, captured by the traps: $P_0 = N_c/\tau_c$. As shown in the inset of Fig. 7, Eq. (1) fits the power dependence of the trap PL measured experimentally reasonably well.

The trapping states can be located either near the conduction band (donors) or near the valence band (acceptors). To separate these cases, we measured the PL and transmission spectra of the samples with different Cd concentrations. The spectra measured at room temperature are shown in Fig. 5(a). The spectra measured for the sample with the $CsPb_{0.55}Cd_{0.45}Br_3$ NCs at T = 11 K are shown in Fig. 8. It is seen that the transmission edge coincides with the exciton PL band. If the trapped states were located in the bandgap near the bottom of the conduction band (donors), the absorption corresponding to optical transitions from the valence band to these states would appear in the spectral range of the wide PL band (traps). However, as shown in Fig. 5(a), no noticeable absorption is observed below the x band for all the samples studied.

We should stress that the transmission spectra are measured for the thick enough samples (d = 0.2 cm) using a Lambda 650 Perkin Elmer spectrophotometer that allows one to detect weak absorption down to $\mu_a d = 0.02$. Correspondingly, the absorption coefficient $\mu_a \leq 0.001$ cm^{-1} that is in many orders of magnitude smaller than that in the range of the interband transitions. This result point out to the negligible concentration of donor centers in the NCs under study. Therefore, we can conclude that the trapped states observed in PL spectra are acceptors.

The PL spectra, as well as the PL QY, are strongly dependent on the sample temperature. Figure 9 shows, as an example, the PL spectra for the sample $CsPb_{0.55}Cd_{0.45}Br_3$ at different temperatures in the range 10–300 K. As seen, the intensity of both the exciton peak and the wide band drop with temperature. In addition, the maximum of A band strongly shifts to the low-energy region, by about 300 meV at T = 120 K. Such a shift cannot be explained by the population of the trap states by the electrons thermally excited from the lower-lying states because their thermal energy $kT \approx 10$ meV that is much smaller than the observed energy shift. The origin of this shift requires further study.

The integral intensity of the full PL shown in the inset of Fig. 9 can be approximated by an Arrhenius-like function,[58]

$$\mathrm{Ar}(T) = \frac{\mathrm{Ar}(0)}{1 + a_1 e^{-\Delta E_1/(kT)} + a_2 e^{-\Delta E_2/(kT)}}, \quad (2)$$

with two activation energies for quenching processes, ΔE_1 = 1.5 meV and ΔE_2 = 52 meV. The physical origin of these processes requires a separate study.

The integral intensity of the wide band, I_A, decreases with temperature faster than that of the PL band, I_X. Figure 10 shows the ratio of the integral intensities, $R(T) = I_X/I_A$. It can be analyzed in the framework of a simple model schematically shown in Fig. 10. We consider a simplified energy structure of an NC consisting of an initial (vacuum) state, "V," two exciton states, "X" and "D," and a wide band, "A," of trapping states (acceptors). Two exciton states are important for the model because one of them (X) is characterized by a relatively short radiative time τ_{XV}.[48,57] We call it the bright (or

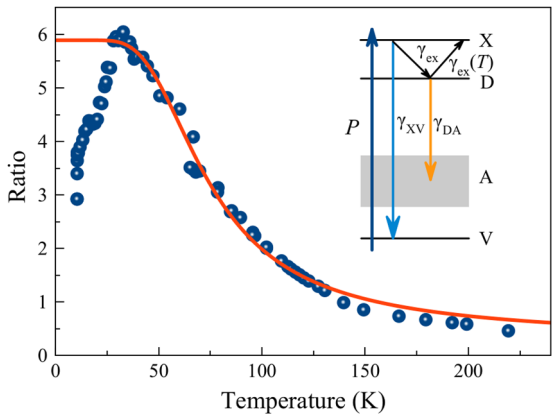

FIG. 10. Temperature dependence of the ratio of integral PL intensity of the wide band and the exciton peak. The solid curve is the fit by Eq. (4). The inset illustrates the model describing this dependence.

02 October 2024 09:37:45

Published under an exclusive license by AIP Publishing

free) exciton state. Another one, the dark (or localized) exciton state (D) radiatively decays very slowly, $\tau_{DV} > 1$ μs, in the $CsPbBr_3$ NCs.[48] This large difference in the relaxation times results in an interesting effect of anti-Stokes PL in $CsPbBr_3$ NCs,[59,60] which is observed at increased temperatures. The physical reason for that is the temperature activated transfer of the dark excitons to the bright states, followed by their rapid relaxation via channel X–V. We use this process to explain the temperature-induced decrease in the ratio of intensities in the $CsPb_{1-x}Cd_xBr_3$ NCs.

We consider several processes in the model. After the optical pumping creating P free excitons per second, the excitons can either radiatively recombine with the rate $\gamma_{XV} = 1/\tau_{XV}$ or relax to the dark state with the rate γ_{ex}. The dark excitons can relax to the trapping states "A," thus creating the wide PL band. At elevated temperatures, the dark excitons can also be excited to the bright state with the rate $\gamma_{ex}(T) = \gamma_{ex} \cdot \exp[-\Delta E/(kT)]$, where the activation energy ΔE is the energy gap between the bright and dark states. For simplicity, we neglect small variation of γ_{ex} due to the Bose-stimulated emission of phonons resonant to transition between the bright and dark exciton states. This process is described by factor $(1 + n)$, where n is the population of phonons with energy $\hbar\omega = \Delta E$. This factor changes γ_{ex} only by about 1.5 times at room temperature that is negligible compared to the change of $\gamma_{ex}(T)$. We ignore the slow process D → V characterized by very long relaxation time τ_{DV} (>1 μs). We also ignore another slow process, X → A. This process can be included in the model; however, the modeling of the ratio $R(T)$ shows that the characteristic time of this process, $\tau_{XA} > 1$ μs, and it does not affect the ratio. The small rates of processes D → V and X → A are probably explained by the strong localization of electron wave functions of the D and A states.

The rate equations describing dynamic processes in the model read

$$\begin{cases} \dfrac{dn_X}{dt} = P - (\gamma_{ex} + \gamma_{XV})n_X + \gamma_{ex}e^{-\Delta E/(kT)}n_D, \\ \dfrac{dn_D}{dt} = \gamma_{ex}n_X - \left(\gamma_{DA} + \gamma_{ex}e^{-\Delta E/(kT)}\right)n_D. \end{cases} \tag{3}$$

Here, n_X and n_D are the populations of states X and D, respectively. Under the steady state excitation conditions, the derivatives in Eq. (3) are zero and the populations are easily obtained from two algebraic equations. The PL intensities of the exciton and additional bands are defined as $I_X = \gamma_{XV} \cdot n_X$ and $I_A = \gamma_{DA} \cdot n_D$. Correspondingly, their ratio, using solution of Eq. (3), is described by the Arrhenius function,

$$R(T) = \frac{A}{1 + ae^{-\Delta E/(kT)}}, \tag{4}$$

where $A = \gamma_{ex}/\gamma_{XV}$ and $a = \gamma_{ex}/\gamma_{DA}$. Fit of the experimentally obtained ratio by this function gives the values $A = 5.9$, $a = 25$, and $\Delta E = 22$ meV. If one assumes that the fast component of the PL decay observed in Ref. 48 is mainly determined by the relaxation rate γ_{ex}, that is, $\tau_{ex} = 1/\gamma_{ex} = 300$ ps, the free exciton radiative lifetime $\tau_{XV} = A \cdot \tau_{ex} \approx 1800$ ps. The characteristic time of the dark exciton radiative relaxation to the trapping states, $\tau_{DA} = a \cdot \tau_{ex} \approx 7500$ ps.

As shown in Fig. 10, the model describes the temperature dependence of the ratio at $T > 30$ K reasonably well. The drop of the ratio at smaller temperatures, which is not described by the model, is explained by the faster PL quenching of the X exciton state compared to that of the D state. This effect is seen in the experiments and it is responsible for the small value of the quenching activation energy, $\Delta E_1 = 1.5$ meV; see Fig. 9 and Eq. (2). At higher temperatures, the quenching channel becomes common for the X and D states so we eliminate them from our consideration when dividing two PL intensities that is calculating the ratio.

The obtained value of the energy gap between the X and D states ($\Delta E = 22$ meV) agrees well with that published in the literature.[48,59,60] The values of relaxation times obtained in the modeling require separate discussion. The radiative lifetime of the X exciton state, $\tau_{XV} \approx 1800$ ps, is hardly possible to measure directly because the radiative process competes with the nonradiative relaxation to the D state and with a quenching process. The radiative lifetime of the D exciton state, $\tau_{DA} \approx 7500$ ps, can be, in principle, measured if the PL quenching processes are not too fast. At present, there is no information about this relaxation time. From a physical point of view, the obtained value of τ_{DA} is unexpectedly short compared to the recombination time of D exciton in the undoped $CsPbBr_3$ NCs ($\tau_{DA} > 1$ μs). In the latter case, the long recombination time is caused by poor overlap of the wave function of the D electron localized near the NC surface with that of the free hole distributed over the NC volume. Therefore, the relatively small value of τ_{DA} in $CsPb_{1-x}Cd_xBr_3$ points out to strong overlap of wave functions of the D electron and trapping centers. This is possible if the trapping centers are mainly localized near the NC surface also.

Similar behavior of PL intensities is observed for the samples with NCs $CsPb_{0.81}Cd_{0.19}Br_3$ and $CsPb_{0.67}Cd_{0.33}Br_3$ (Fig. 10). From the fitting of the temperature dependencies by Eq. (4), the values of model parameters are obtained. With increasing Cd concentration, the free exciton radiative lifetime τ_{XV} increases and the characteristic time τ_{DA} of radiative relaxation of the dark exciton to the trapping states decreases. The obtained values are: $\tau_{XV} = 50$, 350, and 1800 ps; $\tau_{DA} = 15\,000$, 13 000, and 7500 ps for the samples with CdF_2/PbF_2 ratio of 1/10, 2/10, and 3/10, respectively. These results show that with the increase in cadmium concentration, the intensity of the wide band increases, which is explained by an increase in the relaxation rate from the donor center to the acceptor center. This is due to the Cd-induced increase inthe acceptor concentration.

IV. CONCLUSION

In summary, we have carried out the systematic investigation of $CsPb_{1-x}Cd_xBr_3$ perovskite nanocrystals (NCs) by chemical-analytical, x-ray, and optical methods. The x-ray patterns show that NCs with Cd^{2+} ions are successfully formed in the fluorophosphate glass matrix that is confirmed by the shift of the diffraction peaks to larger angles due to change in the lattice constant.

The low-temperature photoluminescence (PL) measurements for the set of the samples with $CsPb_{1-x}Cd_xBr_3$ NCs show the high-energy shift of the exciton PL band with increasing the Cd^{2+} ions concentration. In addition, the low temperature PL spectra contain an additional wide band in the range of 1.6–2.2 eV. It is shown that this band corresponds to optical transitions to the deep acceptor states. Partial substitution of the B-site (Pb^{2+}) cation by ions

02 October 2024 09:37:45

Published under an exclusive license by AIP Publishing

with smaller radius, in our case by the cadmium ions, leads to the formation of new deep defect states destroying the defect tolerance property of the host $CsPbBr_3$. These new defect states act as traps and scattering centers, hampering the optoelectronic performance and radically reducing the PL quantum yield (QY) down to 4%–5% at room temperature for high concentration of Cd^{2+} ions. The decrease in the QY is accompanied by a shift of the absorption band toward higher energies of up to 2.64 eV, which makes it possible to create blue glass phosphors with cadmium containing NCs. In particular, the PL QY of NCs $CsPb_{0.81}Cd_{0.19}Br_3$ is 21% at the emission energy of 2.56 eV (wavelength 484 nm) that is still larger than that for the case of anion exchange, namely, for $CsPb(Br,Cl)_3$ NCs, in which the QY is 13% at the same emission energy.

ACKNOWLEDGMENTS

M.S.K. and I.V.I. acknowledge the financial support from St. Petersburg State University (Grant No. 122040800257-5) for the experimental part of this work. The TEM image was carried out using equipment of the Resource Center "Nanotechnology" of the SPbSU Research Park.

AUTHOR DECLARATIONS

Conflict of Interest

The authors have no conflicts to disclose.

Author Contributions

Conceptualization, M.S.K., E.V.K., and I.V.I.; methodology, M.S.K., E.V.K., M.N.B., V.S.B, E.V.U., and I.V.I.; validation, M.S.K., E.V.K., M.N.B., D.V.P., M.B.S., and I.V.I.; investigation, M.S.K., M.N.B., V.S.B, E.V.U., and I.V.I.; writing—original draft preparation, M.S.K., E.V.K., and I.V.I.; supervision, M.S.K., E.V.K., and I.V.I.; project administration, M.S.K., E.V.K., and I.V.I.; funding acquisition, M.S.K., and I.V.I. All authors have read and agreed to the published version of the manuscript.

Maria S. Kuznetsova: Conceptualization (equal); Funding acquisition (equal); Investigation (equal); Methodology (equal); Project administration (equal); Supervision (equal); Validation (equal); Writing – original draft (equal). **Elena V. Kolobkova**: Conceptualization (equal); Methodology (equal); Project administration (equal); Supervision (equal); Validation (equal); Writing – original draft (equal). **Matvey N. Bataev**: Investigation (equal); Methodology (equal); Validation (equal). **Vladimir S. Berdnikov**: Investigation (equal); Methodology (equal). **Dmitrii V. Pankin**: Validation (equal); Writing – original draft (equal). **Mikhail B. Smirnov**: Methodology (equal); Validation (equal). **Evgenii V. Ubyivovk**: Investigation (equal); Methodology (equal). **Ivan V. Ignatiev**: Conceptualization (equal); Funding acquisition (equal); Investigation (equal); Methodology (equal); Project administration (equal); Supervision (equal); Validation (equal); Writing – original draft (equal).

DATA AVAILABILITY

The data that support the findings of this study are available from the corresponding author upon reasonable request.

REFERENCES

[1] B. R. Sutherland and E. H. Sargent, Nat. Photonics **10**, 295 (2016).
[2] L. C. Schmidt, A. Pertegas, S. González-Carrero, O. Malinkiewicz, S. Agouram, G. Mínguez Espallargas, H. J. Bolink, R. E. Galian, and J. Pérez-Prieto, J. Am. Chem. Soc. **136**, 850–853 (2014).
[3] B. Yang, J. Chen, F. Hong, X. Mao, K. Zheng, S. Yang, Y. Li, T. Pullerits, W. Deng, and K. Han, Angew. Chem., Int. Ed. **56**, 12471–12475 (2017).
[4] Y. Fu, H. Zhu, A. W. Schrader, D. Liang, Q. Ding, P. Joshi, L. Hwang, X. Zhu, and S. Jin, Nano Lett. **16**, 1000–1008 (2016).
[5] H. Cho, S.-H. Jeong, M.-H. Park, Y.-H. Kim, C. Wolf, C.-L. Lee, J. H. Heo, A. Sadhanala, N. Myoung, S. Yoo, S. H. Im, R. H. Friend, and T.-W. Lee, Science **350**, 1222–1225 (2015).
[6] R. S. Sanchez, M. S. de la Fuente, I. Suarez, G. Muñoz-Matutano, J. P. Martinez-Pastor, and I. Mora-Sero, Sci. Adv. **2**, e1501104 (2016).
[7] Z.-K. Tan, R. S. Moghaddam, M. L. Lai, P. Docampo, R. Higler, F. Deschler, M. Price, A. Sadhanala, L. M. Pazos, D. Credgington, F. Hanusch, T. Bein, H. J. Snaith, and R. H. Friend, Nat. Nanotechnol. **9**, 687–692 (2014).
[8] L. Protesescu, S. Yakunin, M. I. Bodnarchuk, F. Krieg, R. Caputo, C. H. Hendon, R. X. Yang, A. Walsh, and M. V. Kovalenko, Nano Lett. **15**, 3692–3696 (2015).
[9] S. Yakunin, L. Protesescu, F. Krieg, M. I. Bodnarchuk, G. Nedelcu, M. Humer, G. De Luca, M. Fiebig, W. Heiss, and M. V. Kovalenko, Nat. Commun. **6**, 8056 (2015).
[10] Q. A. Akkerman, M. Gandini, F. Di Stasio, P. Rastogi, F. Palazon, G. Bertoni, J. M. Ball, M. Prato, A. Petrozza, and L. Manna, Nat. Energy **2**, 16194 (2016).
[11] Y. Tong, E. Bladt, M. F. Aygüler, A. Manzi, K. Z. Milowska, V. A. Hintermayr, P. Docampo, S. Bals, A. S. Urban, and L. Polavarapu, Angew. Chem., Int. Ed. **55**, 13887–13892 (2016).
[12] G. Raino, G. Nedelcu, L. Protesescu, M. I. Bodnarchuk, M. V. Kovalenko, R. F. Mahrt, and T. Stoferle, ACS Nano **10**, 2485–2490 (2016).
[13] Q. A. Akkerman, S. G. Motti, A. R. Srimath Kandada, E. Mosconi, V. D'Innocenzo, G. Bertoni, S. Marras, B. A. Kamino, L. Miranda, F. De Angelis, A. Petrozza, M. Prato, and L. Manna, J. Am. Chem. Soc. **138**, 1010–1016 (2016).
[14] J. Kang and L.-W. Wang, J. Phys. Chem. Lett. **8**(2), 489–493 (2017).
[15] Y. Su, X. Chen, W. Ji, Q. Zeng, Z. Ren, Z. Su, and L. Liu, ACS Appl. Mater. Interfaces **9**, 33020–33028 (2017).
[16] M. Imran, V. Caligiuri, M. Wang, L. Goldoni, M. Prato, R. Krahne, L. De Trizio, and L. Manna, J. Am. Chem. Soc. **140**, 2656–2664 (2018).
[17] A. Knight and L. M. Herz, Energy Environ. Sci. **13**, 2024–2046 (2020).
[18] S. T. Ochsenbein, F. Krieg, Y. Shynkarenko, G. Raino, and M. V. Kovalenko, ACS Appl. Mater. Interfaces **11**, 21655–21660 (2019).
[19] G. Nedelcu, L. Protesescu, S. Yakunin, M. I. Bodnarchuk, M. J. Grotevent, and M. V. Kovalenko, Nano Lett. **15**, 5635 (2015).
[20] M. C. Weidman, M. Seitz, S. D. Stranks, and W. A. Tisdale, ACS Nano **10**, 7830 (2016).
[21] W. van der Stam, J. J. Geuchies, T. Altantzis, K. H. W. van den Bos, J. D. Meeldijk, S. Van Aert, S. Bals, D. Vanmaekelbergh, and C. de Mello Donega, J. Am. Chem. Soc. **139**, 4087–4097 (2017).
[22] I. D. Skurlov, W. Yin, A. O. Ismagilov, A. N. Tcypkin, H. Hua, H. Wang, X. Zhang, A. P. Litvin, and W. Zheng, Nanomaterials **12**(1), 151 (2022).
[23] R. Begum, M. R. Parida, A. L. Abdelhady, B. Murali, N. M. Alyami, G. H. Ahmed, M. N. Hedhili, O. M. Bakr, and O. F. Mohammed, J. Am. Chem. Soc. **139**, 731–737 (2017).
[24] H. Shao, X. Bai, H. Cui, G. Pan, P. Jing, S. Qu, J. Zhu, Y. Zhai, B. Dong, and H. Song, Nanoscale **10**, 1023–1029 (2018).
[25] N. Mondal, A. De, and A. Samanta, ACS Energy Lett. **4**, 32–39 (2019).
[26] Z. J. Yong, S. Q. Guo, J. P. Ma, J. Y. Zhang, Z. Y. Li, Y. M. Chen, B. B. Zhang, Y. Zhou, J. Shu, J. L. Gu, L. R. Zheng, O. M. Bakr, and H. T. Sun, J. Am. Chem. Soc. **140**, 9942–9951 (2018).

02 October 2024 09:37:45

Published under an exclusive license by AIP Publishing

[27]Z. J. Li, E. Hofman, A. H. Davis, A. Khammang, J. T. Wright, B. Dzikovski, R. W. Meulenberg, and W. Zheng, Chem. Mater. **30**, 6400–6409 (2018).
[28]G. Pan, X. Bai, D. Yang, X. Chen, P. Jing, S. Qu, L. Zhang, D. Zhou, J. Zhu, W. Xu, B. Dong, and H. Song, Nano Lett. **17**, 8005–8011 (2017).
[29]J. S. Yao, J. Ge, B. N. Han, K. H. Wang, H. B. Yao, H. L. Yu, J. H. Li, B. S. Zhu, J. Z. Song, C. Chen, Q. Zhang, H. B. Zeng, Y. Luo, and S. H. Yu, J. Am. Chem. Soc. **140**, 3626–3634 (2018).
[30]T. He, J. Li, C. Ren, S. Xiao, Y. Li, R. Chen, and X. Lin, Appl. Phys. Lett. **111**, 211105 (2017).
[31]L. Fei, X. Yuan, J. Hua, M. Ikezawa, R. Zeng, H. Li, Y. Masumoto, and J. Zhao, Nanoscale **10**, 19435–19442 (2018).
[32]D. Chen, S. Zhou, F. Tian, H. Ke, N. Jiang, S. Wang, Y. Peng, and Y. Liu, Adv. Opt. Mater. **7**, 1901082 (2019).
[33]A. Swarnkar, W. Mir, and A. Nag, ACS Energy Lett. **3**, 286–289 (2018).
[34]G. H. Ahmed, J. Yin, O. M. Bakr, and O. F. Mohammed, J. Chem. Phys. **152**(2), 020902 (2020).
[35]C. Xie, Y. Zhao, W. Shi, and P. Yang, Langmuir **37**, 1183–1193 (2021).
[36]K. Wei, P. Li, Y. Duan, S. Zhang, L. Chen, S. Xu, and J. Zhang, J. Non-Cryst. Solids **570**, 121022 (2021).
[37]L. Niu, H. Shi, Y. Ye, C. Liu, B. Jia, Y. Chu, L. Liu, J. Ren, and J. Zhang, J. Non-Cryst. Solids **581**, 121429 (2022).
[38]Y. Zhou, C. Liu, Z. Zhao, W. Zhang, K. Li, Y. Ye, C. F. Zhu, and X. G. Meng, J. Alloys Compd. **827**, 154349 (2020).
[39]M. Hao, Q. Wang, J. Li, W. Xiang, H. Fan, and X. Liang, Mater. Today Chem. **26**, 101020 (2022).
[40]J. Liu, S. Liu, Y. Chen, Q. Zhao, Y. Zhao, W. Xiang, X. Liang, and B. Ren, Ceram. Int. **45**, 22688–22693 (2019).
[41]Z. Zhang, M. Wang, Y. Liu, J. Zhang, J. Wang, J. Han, C. Liu, and J. Ruan, Ceram. Int. **48**, 17596–17603 (2022).
[42]Y. Zhao, C. Shen, L. Ding, J. Liu, W. Xiang, and X. Liang, Opt. Mater. **107**, 110046 (2020).
[43]E. V. Kolobkova, A. A. Lipovskii, V. D. Petrikov, and V. G. Melekhin, Glass Phys. Chem. **28**(4), 251–255 (2002).
[44]E. Kolobkova, Z. Lipatova, and A. Abdrshin, and N. Nikonorov, Opt. Mater. **65**, 124–128 (2017).
[45]A. A. Lipovskii, I. E. Yakovlev, E. V. Kolobkova, and V. D. Petrikov, J. Eur. Ceram. Soc. **19**(6–7), 865–869 (1999).
[46]E. V. Kolobkova, M. S. Kuznetsova, and N. V. Nikonorov, J. Non-Cryst. Solids **563**, 120811 (2021).
[47]E. V. Kolobkova, R. Semaan, M. S. Kuznetsova, and N. V. Nikonorov, J. Lumin. **255**, 119541 (2023).
[48]V. V. Belykh, M. L. Skorikov, E. V. Kulebyakina, E. V. Kolobkova, M. S. Kuznetsova, M. M. Glazov, and D. R. Yakovlev, Nano Lett. **22**(11), 4583–4588 (2022).
[49]E. Kirstein, N. E. Kopteva, D. R. Yakovlev, E. A. Zhukov, E. V. Kolobkova *et al.*, Nat. Commun. **14**(1), 699 (2023).
[50]D. Liu, H. Peng, and R. Sa, Comput. Theor. Chem. **1200**, 113251 (2021).
[51]N. O. Damerdji, B. Amrani, K. D. Khodja, and P. Aubert, J. Supercond. Novel Magn. **31**, 2935–2940 (2018).
[52]S. J. Clark, M. D. Segall, C. J. Pickard, P. J. Hasnip, M. J. Probert, K. Refson, and M. C. Payne, Z. Kristallogr. **220**, 567–570 (2005).
[53]K. Refson, P. R. Tulip, and S. J. Clark, Phys. Rev. B **73**(15), 155114 (2006).
[54]J. Aarons, A new CASTEP and ONETEP geometry optimiser, 2011, http://www.hector.ac.uk/cse/distributedcse/reports/castep-geom/castep-geom/HTML/dCSE_project.html.
[55]H. J. Monkhorst and J. D. Pack, Phys. Rev. B **13**, 5188 (1976).
[56]J. A. Peters, Z. Liu, R. Yu, K. M. McCall, Y. He, M. G. Kanatzidis, and B. W. Wessels, Phys. Rev. B **100**, 235305 (2019).
[57]A. V. Mikhailov, A. S. Kurdyubov, E. S. Khramtsov, I. V. Ignatiev, B. F. Gribakin, S. Cronenberger, D. Scalbert, M. R. Vladimirova, and R. Andre, Semiconductors **57**, 586 (2024); arXiv:2304.07135.
[58]A. V. Trifonov, S. N. Korotan, A. S. Kurdyubov, I. Y. Gerlovin, I. V. Ignatiev, Y. P. Efimov, S. A. Eliseev, V. V. Petrov, Y. K. Dolgikh, V. V. Ovsyankin, and A. V. Kavokin, Phys. Rev. B **91**, 115307 (2015).
[59]M. A. Becker, R. Vaxenburg, G. Nedelcu, P. C. Sercel, A. Shabaev, M. J. Mehl, J. G. Michopoulos, S. G. Lambrakos, N. Bernstein, J. L. Lyons, T. Stöferle, R. F. Mahrt, M. V. Kovalenko, D. J. Norris, G. Rainò, and A. L. Efros, Nature **553**, 189–193 (2018).
[60]M. S. Kuznetsova, M. N. Bataev, M. A. Chukeev, N. D. Rostovtsev, S. Y. Verbin, I. V. Ignatiev, V. Y. Davydov, A. N. Smirnov, I. A. Eliseev, and E. V. Kolobkova, Opt. Spectrosc. **130**(11), 1472 (2022).

02 October 2024 09:37:45

Published under an exclusive license by AIP Publishing